BAAA, Vol. 60, 2018
P. Benaglia, A.C. Rovero, R. Gamen & M. Lares, eds.

Asociación Argentina de Astronomía
Boletín de artículos científicos

Instabilities, shocks and turbulence in space and astrophysical plasmas

D. O. Gómez[1,2]

[1] *Instituto de Astronomía y Física del Espacio, CONICET–UBA, Argentina*
[2] *Departamento de Física, FCEN–UBA, Argentina*

Contact / gomez@iafe.uba.ar

Resumen / Los plasmas que componen el medio interplanetario e interestelar son habitualmente descriptos en el marco de la magnetohidrodinámica (MHD), con el consiguiente acoplamiento entre flujos y campos magnéticos. Este marco teórico modela satisfactoriamente el comportamiento de gran escala de varios de los procesos que tienen lugar en dichos plasmas, tales como la generación de campos magnéticos por efecto dínamo, la impulsiva liberación de energía magnética en eventos de reconexión o la compleja dinámica de los flujos turbulentos. Sin embargo, a escalas espaciales más pequeñas se observan fenómenos que no han podido explicarse en el marco de la MHD tradicional. A lo largo del presente trabajo veremos que incorporando efectos adicionales tales como la corriente de Hall y la inercia de los electrones, es posible describir algunos de estos fenómenos, tales como la estructura fina de algunos *shocks* espaciales o las desviaciones observadas recientemente en el espectro de la turbulencia del viento solar.

Abstract / The dynamics of plasmas pervading the interplanetary and interstellar medium are often described within the frame of magnetohydrodynamics (MHD), which involves the coupling between flows and magnetic fields. This theoretical framework adequately models the large scale behavior of a number of processes taking place in these plasmas, such as the generation of magnetic fields by dynamo mechanisms, the impulsive release of magnetic energy in reconnection events or the complex dynamics of turbulent flows. However, there are physical phenomena at smaller spatial scales that cannot be explained within the framework of traditional MHD. Throughout this work we show that the inclusion of additional physical effects such as the Hall current or electron inertia, it becomes possible to describe phenomena such as the fine structure of some shocks or the recently observed deviations in the turbulent energy spectrum of the solar wind.

Keywords / plasmas — instabilities — shock waves — turbulence

1. Introduction

One-fluid magnetohydrodynamics (MHD) provides a reasonable description for relatively large-scale phenomena observed in space and astrophysical plasmas. For instance, the dynamics and heating of the plasma confined in coronal loops, has been thoroughly studied within the framework of one-fluid MHD (Gómez, 1990). Another example is the observation of patterns consistent with the occurrence of MHD instabilities, such as Rayleigh-Taylor in connection with supernova remnants (Velazquez et al., 1998), or Kelvin-Helmholtz in coronal mass ejections. In fact, high resolution images obtained by the *Atmospheric Imaging Assembly* (AIA) on board the *Solar Dynamics Observatory* (SDO) reveal the unfolding of the Kelvin-Helmholtz instability, as coronal mass ejections expand in the ambient corona. In particular, for the 2010 November 3 event (Foullon et al., 2011), a large-scale magnetic field mostly tangential to the interface is inferred, while the magnetic field component along the shear flow is not strong enough to quench the instability (see also Ofman & Thompson 2011 for a 2010 April 8 event). Also, there is compelling observational evidence indicating that the ambient corona is in a small-scale turbulent regime (based on the nonthermal broadening of spectral lines), and therefore the criteria for the development of the instability are a-priori expected to differ from the laminar case. In view of these observational findings, we decided to numerically study the evolution of the Kelvin-Helmholtz instability with a turbulent background, by performing three-dimensional simulations of the magnetohydrodynamic equations (Gómez et al., 2016). The instability is driven by a velocity profile tangential to the CME-corona interface, which we simulate through a hyperbolic tangent profile, while the turbulent background is generated by the application of a stationary stirring force. These results are presented in §2..

The sustained improvement in cadence and spatial resolution of astronomical and space instruments led to the observation of physical processes taking place at smaller scales. As we move to smaller spatial and temporal scales, one-fluid MHD might become insufficient to describe some of the physics observed on space and astrophysical plasmas. When the ion inertial scale becomes non-negligible, the Hall effect must be included, giving rise to a Hall-MHD description (Gómez et al., 2013) (see also Gómez et al. 2008 for plasmas embedded in strong magnetic fields). One of the environments where new physical effects have actually been

observed and are being actively studied, is the solar wind turbulence. For instance, Sahraoui et al. (2009) obtained clear evidence of two break points in the magnetic energy spectra observed by the multi-spacecraft Cluster mission. These break points are inconsistent with the traditional MHD description, which predicts a single power law spectrum (Kolmogorov-like) all the way down to dissipative scales. Multi-fluid models represent a step forward with respect to one-fluid MHD and also Hall-MHD, incorporating new physical effects along with new spatial and temporal scales. We have recently presented a two-fluid MHD description (Andrés et al., 2014b) which retains the effects of the Hall current, electron pressure and electron inertia. According to this two-fluid description, ions and electrons introduce their inertial length scales λ_i and λ_e, which are not present in one-fluid MHD. We performed numerical simulations of the two-fluid MHD equations, and observe that the magnetic energy spectrum indeed shows two break points at wavenumbers associated with spatial scales λ_i and λ_e. In §3. we show these numerical results and discuss the connection with the magnetic energy spectrum derived from in-situ measurements.

Another example where the two-fluid MHD framework seems appropriate, is in the description of collisionless shocks. The dynamics of the large-scale regions upstream and downstream from the shock, is presumably well described by one-fluid MHD. The structure of the shock itself, however, is determined by collisionless processes at much smaller spatial scales. Therefore, the inertial scale of the particle species involved is expected to play a role. In §4. we show results from one-dimensional simulations of the two-fluid equations, showing that the electron inertial scale does indeed determine the ramp thickness of perpendicular collisionless shocks.

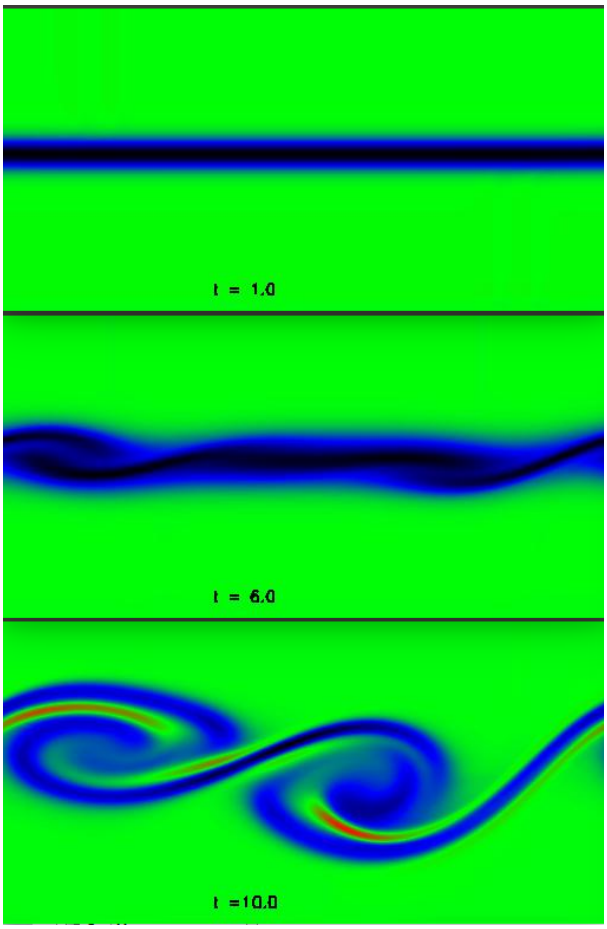

Figure 1: Vorticity $\omega_z(x, y)$ at three successive times, as labelled. Green corresponds to $\omega_z = 0$, while black (red) corresponds to negative (positive) values.

2. Kelvin-Helmholtz instability in coronal mass ejections

The MHD equations for a fully ionized plasma in the incompressible limit are

$$\frac{\partial \boldsymbol{U}}{\partial t} = -\left(\boldsymbol{U}\cdot\nabla\right)\boldsymbol{U} + v_A^2\left(\nabla\times\boldsymbol{B}\right)\times\boldsymbol{B} - \nabla P + \nu\nabla^2\boldsymbol{U} + \boldsymbol{F}\ , \quad (1)$$

$$\frac{\partial \boldsymbol{B}}{\partial t} = \nabla\times\left(\boldsymbol{U}\times\boldsymbol{B}\right) + \eta\nabla^2\boldsymbol{B}\ , \quad (2)$$

$$\nabla\cdot\boldsymbol{B} = 0 = \nabla\cdot\boldsymbol{U}\ . \quad (3)$$

The velocity $\boldsymbol{U}$ is expressed in units of a characteristic speed U_0, the magnetic field $\boldsymbol{B}$ is in units of B_0, and we also assume a characteristic length scale L_0 and a spatially uniform particle density n_0. The (dimensionless) Alfven speed is then $v_A = B_0/\sqrt{4\pi m_i n_0}U_0$, while η and ν are respectively the dimensionless magnetic diffusivity and kinematic viscosity.

Numerical simulations have progressively become an important tool for the study of plasma flows. Over the years, we developed a diversity of parallel codes based on pseudo-spectral methods aimed at speeding up large Reynolds number simulations (Gómez et al., 2005). One of the features of the simulations reported here, is to maintain a hyperbolic tangent profile $U_y(x) = U_0\tanh(\frac{x}{\Delta})$, which will drive the Kelvin-Helmholtz instability with a growth rate γ_{KH}

$$\left(\frac{\gamma_{KH}\Delta}{U_0}\right)^2 = \frac{1}{4}\left(e^{-4k\Delta} - (2k\Delta - 1)^2\right). \quad (4)$$

The time evolution of the vorticity component $\omega_z(x, y, t)$ is shown in Fig. 1, which displays the well known K-H pattern. Green corresponds to $\omega_z = 0$, while black (red) corresponds to negative (positive) values of the vorticity component ω_z.

As mentioned, we superimpose a small-scale turbulent background in our simulations. We do this by applying a stationary force to all modes within a thin spherical shell of radius $k_{turb} = 1/l_{turb}$ in Fourier space. The nonlinear interactions between these Fourier modes being externally driven with a force of intensity f_{turb}, will develop a stationary turbulent regime with an energy cascade that involves all wavenumbers $k \geq k_{turb}$. We choose l_{turb} to be much smaller than the wavelength observed for the KH pattern, and even somewhat smaller than the thickness Δ of the shear layer

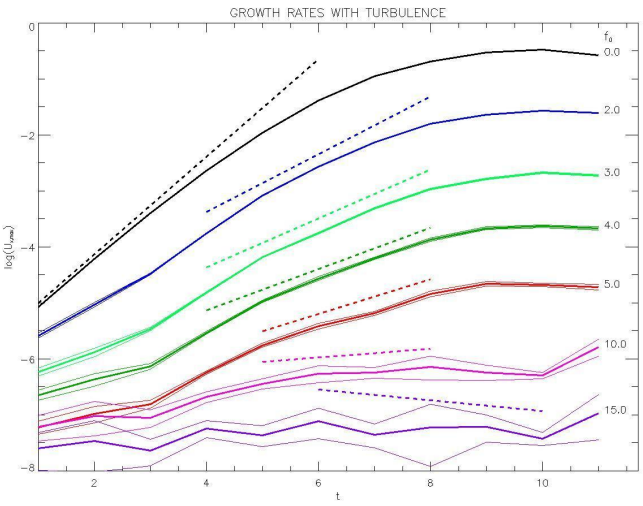

Figure 2: Maximum U_x vs. time in a lin-log plot for different turbulence intensities (labelled). Dotted lines correspond to the theoretical growth rate.

(i.e. $l_{turb} < \Delta$).

In Fig. 2 we superimpose the maximum value of $U_x(x, y)$ vs. time for several runs with different values of intensity for the turbulent background. Since it is a lin-log plot, the straight line fit provides the growth rate for each run.

The expected effect of the small-scale turbulence on the large scale instability, is an effective or enhanced diffusivity. As a result, the modified instability growth rate is expected to be

$$\gamma(k) = \gamma_{KH}(k) - \nu_{turb} k^2 \ , \tag{5}$$

where $\gamma_{KH}(k)$ is given in Eq. (4) and ν_{turb} is an effective or turbulent viscosity. On dimensional arguments, the turbulent viscosity introduced in Eq. (5) should depend on the turbulence parameters f_{turb} and l_{turb} like

$$\nu_{turb} = 18.8 \ (f_{turb} \ l_{turb}^3)^{1/2} \ , \tag{6}$$

where the numeric factor is the best fit to our simulations.

Kelvin-Helmholtz is a well-known macroscopic and ideal shear-driven instability, but certainly not the only one. In low-density plasmas, for which the Hall effect becomes non-negligible, the so-called *Hall magnetoshear* instability can also take place. Gómez et al. (2014) performed three-dimensional simulations of the Hall-MHD equations where these two shear-driven instabilities are present. The main result from this study is that when the shear flow is so intense that its vorticity surpasses the ion-cyclotron frequency, the Hall magnetoshear instability becomes more important than Kelvin-Helmholtz. The Hall magnetoshear instability might be important on highly sheared astrophysical flows, such as near the boundaries of astrophysical jets. It should not be confused with the well known *Magneto-Rotational* instability (Gómez, 2009), which takes place in accretion disks, since the magnetoshear instability does not require a rotating flow to occur.

3. Two-fluid turbulence in the solar wind

We use a standard parallel pseudospectral code to evaluate the nonlinear terms and numerically integrate the two-fluid MHD or EIHMHD (Electron Inertia Hall MHD) equations (see details in Andrés et al. 2014b). A second-order Runge-Kutta time integration scheme is used. Periodic boundary conditions are assumed in both directions of a square box and no external forcing is applied. Initial conditions are non-zero for all Fourier modes in a shell in k-space where $3 \leq k \leq 4$. For the run shown in Fig. 3 spatial resolution is 1024^2 grid points, $\lambda_i = 0.1$ and the mass ratio is $(m_i + m_e)/m_e = 25$. The inertial scales are then $\lambda_{i,e} = c/\omega_{i,e}$, where $\omega_{i,e}$ is the ion and electron plasma frequency. The wavenumbers $k_{\lambda_{i,e}}$ associated to the inertial scales are simply $k_{\lambda_{i,e}} = 1/\lambda_{i,e}$.

The code is run for sufficiently long times, until a quasi-stationary turbulent regime is established. In Andrés et al. (2014b) we have discussed how the presence of the inertial lengthscales causes the appearance of three different regions in wavenumber space, characterized by different slopes in the magnetic energy power spectrum:

- MHD region ($k < 1/\lambda_i$): In this region $E_k \simeq B_k^2/k \simeq \epsilon^{2/3} k^{-5/3}$.
- Hall-MHD region ($1/\lambda_i < k < 1/\lambda_e$): In this intermediate region $E_k \simeq B_k^2/k \simeq (\epsilon/\lambda)^{2/3} k^{-7/3}$.
- Electron-dominated region ($1/\lambda_e < k$): In this large-k region is $B_k^2/k \simeq (\epsilon/(\delta\lambda^3))^{2/3} k^{-11/3}$.

In these expresions, ϵ is the total energy dissipation rate characterizing the quasi-stationary turbulent regime, $\lambda = c/\omega_M$ and $\delta = m_e/M$, where $M = m_i + m_e$. These slopes are derived from a dimensional analysis performed on the nonlinear energy flow in wavenumber space. They are also rigorously supported by the von Karman-Howarth equation (von Karman & Howarth, 1938) associated to a two-fluid MHD description, as recently shown by Andrés et al. (2016b). In the paradigmatic case of incompressible hydrodynamic turbulence, the von Karman-Howarth equation is one of the cornerstones of turbulence theory, relating the time evolution of the second-order correlation velocity tensor to the divergence of the third-order correlation velocity tensor. This important result has been extended to one-fluid MHD turbulent plasmas, and also to include the Hall effect. Recently, Andrés et al. (2016b) extended its validity to two-fluid MHD turbulence, and the previous results can be regarded as particular cases in the proper asymptotic limits.

The two break points observed in our simulations, respectively at k_{λ_i} and k_{λ_e}, suggest that the spectra observed by Sahraoui et al. (2009) might be explained within the framework of two-fluid MHD. This is still a matter of debate, since at scales as small as the electron inertial length, other kinetic effects are important and might play a role in shaping up the spectrum.

In a related study (Andrés et al., 2016a), we also found that two-fluid MHD produces significant departures from one-fluid MHD in magnetic reconnection events. The traditional Sweet-Parker model for magnetic reconnection (Parker, 1957) relies on Joule dissipation to reconnect field lines and it is far too ineficient for

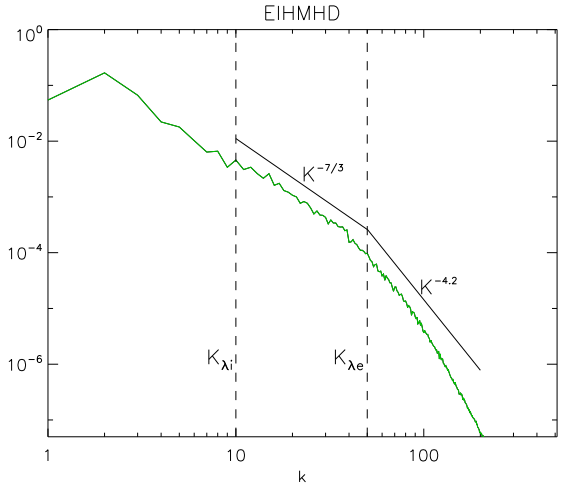

Figure 3: Power spectrum of magnetic energy for a two-dimensional EIHMHD simulation with $\lambda_i = 0.1$ and $M/m_e = 25$.

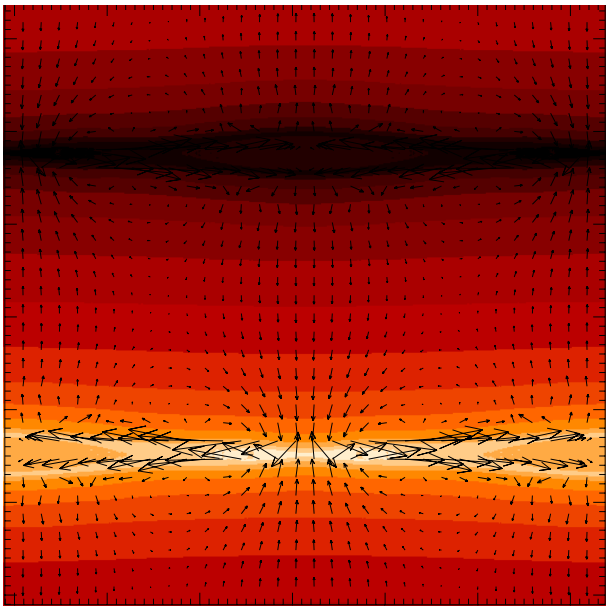

Figure 4: Current density $j_z(x, y)$ showing positive (white) and negative (black) current sheets. The arrows show the electron velocity field.

most space and astrophysical plasma situations. However, when the inertial scales are larger than the dissipative Joule scale, two-fluid effects should be considered. Our simulations show that the thickness of the current sheet during reconnection is as thin as the electron inertial scale, and the reconnection rate scales with the ion inertial length (see also Andrés et al. 2014a). Fig. 4 shows the distribution of current density $j_z(x, y)$, displaying a positive (negative) current sheet in white (black). Overlaid, the arrows illustrate the velocity of electrons approaching the reconnection sites from above and below, and flowing out at the sides at superalfvenic speeds. In particular, this reconnection regime qualifies as fast reconnection, since the reconnection rate becomes independent of the plasma electric resistivity.

4. Two-fluid model of perpendicular shocks

Shocks are ubiquitous in space and astrophysical plasmas, and transform the kinetic energy of the flow into thermal energy and particle acceleration. The details of this energy transfer are not completely understood, but it is a multiscale process related to the spatial and temporal structure of the electromagnetic fields within the inner shock structure. In low density plasmas, the mean free path of particles becomes much larger than the shock thickness, and therefore particle collisions play no role in the shock structure.

Perpendicular shocks (i.e. those for which the magnetic field remains tangential to the shock) are particularly interesting, since magnetic pressure causes them to behave quite differently from hydrodynamic shocks. Schwartz et al. (2011) have recently obtained that the thickness of the Earth bow shock is only a few electron inertial lengths, from in-situ observations performed by the four Cluster spacecrafts (see also Mazelle et al. 2010).

Following the one-dimensional model for plasma solitons sketched by Balogh & Treumann (2013), we derived one-dimensional two-fluid equations to study the dynamics of waves propagating in directions perpendicular to the magnetic field. In this simplified one-dimensional geometry, only the fast magnetosonic mode is able to propagate. We therefore performed simulations to follow the propagation of a finite amplitude fast magnetosonic wave to study the generation of fast magnetosonic shocks as well as their internal structure once they are formed. The initially sinusoidal profile evolves in time into a shock, as shown in Fig. 5 for the particle density ($n_e = n_i$ due to quasi-neutrality), the parallel velocity (in the direction of propagation), the perpendicular (i.e. tangent to the shock) electron velocity ($u_{\perp,i} = -(m_e/m_i)u_{\perp,e}$), the (perpendicular) magnetic field, as well as the parallel and perpendicular components of the electric field. All these profiles propagate to the right in the periodic box, displaying a shock at the front and a trailing magnetosonic wave in the "shocked" region. The electric field component along the magnetic field is particularly interesting, since it is the component responsible of accelerating individual particles. However, the acceleration process itself is beyond the scope of a fluidistic description, as the one presented here.

To study the structure of the shock ramp, we performed simulations with different values of the mass ratio M/m_e. In Fig. 6 we show the parallel velocity profile $U_x(x)$ for different mass ratios (labelled) at a fixed time

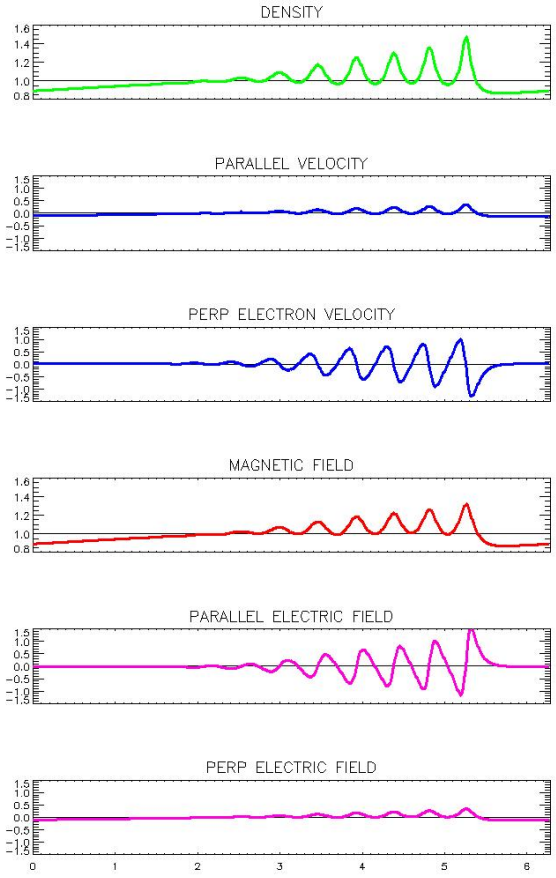

Figure 5: Profiles of the various fields accross the shock direction for $M/m_e = 100$.

where the shock ramp has formed and propagates unchanged. The dark blue trace indicates the ramp portion of each profile. We obtain that the thickness of the ramp is proportional to the square root of the mass ratio and therefore it correlates with the electron inertial length λ_e. This numerical result is exactly coincident with the observations reported by Schwartz et al. (2011).

5. Conclusions

The dynamics of interplanetary and interstellar plasmas are usually described within the framework of the traditional one-fluid MHD. In this context, we presented recent simulations aimed at modelling the evolution of a large-scale Kelvin-Helmholtz unstable configuration, embedded in a turbulent background. The results arising from these simulations were compared with AIA/SDO images of the solar corona, where a Kelvin-Helmholtz pattern is observed to progress at one of the flanks of a coronal mass ejection. As expected, the role of the turbulent background is to slow down the instability. In order for the observed instability growth rate to match the one arising from our simulations, the background turbulence should indeed have a correlation length of less than 200 km, which is somewhat below

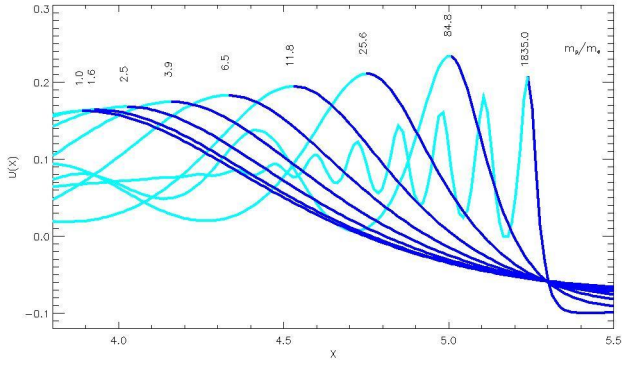

Figure 6: Velocity profile $U_x(x)$ for different mass ratios m_e/m_i as labelled. The dark blue trace shows the shock ramp portion of the profile.

the spatial resolution of present-day instruments. Even though spatially unresolved, this background turbulence is responsible for the nonthermal broadening (of about 60 km/s) of several spectral lines observed in the corona.

On the other hand, one-fluid MHD has its own limitations, since there are physical phenomena at smaller spatial scales that cannot be adequately explained. We showed that within the more general framework of two-fluid MHD, the inclusion of additional physical effects such as the Hall current or electron inertia, it becomes possible to describe some of these phenomena. One of the examples is the small scale structure of the solar wind turbulence. We report magnetic energy spectra arising from two-fluid MHD turbulent simulations, showing break points at the ion and electron inertial scales λ_i and λ_e. The occurrence of these breaks as well as the spectral slopes in each range, are confirmed by elementary dimensional analysis and by the more rigorous arguments based on the von Karman-Howarth equation. Moreover, these numerical results are strikingly similar to those derived from in-situ observations of the solar wind performed by the multi-spacecraft Cluster mission.

Another example where a two-fluid MHD description is expected to be relevant, is in collisionless shocks. Shocks separate two relatively large-scale regions (upstream and downstream), for which a one-fluid MHD description is presumably adequate. However, the internal structure of the shock itself is determined by much smaller spatial scales, which for low density plasmas is not related to collisional processes. The recent observation that the Earth bow shock has a thickness of only a few λ_e, led us to develop a one-dimensional two-fluid MHD model to follow the propagation and nonlinear dynamics of finite amplitude fast magnetosonic waves. Our simulations have shown that fast magnetosonic waves propagating perpendicular to the magnetic field not only evolve to form shocks, but also that once these shocks are formed, their ramp thicknesses are of the order of a few electron inertial length scales.

In summary, we have seen a few examples where magnetohydrodynamics have been used to describe the behavior of space and astrophysical plasmas. Although one-fluid MHD is often appropriate for the large-scale

behavior, at smaller spatial scales two-fluid MHD provides a reasonable theoretical description for new physical phenomena. However, it is important to emphasize that there are a number of purely kinetic plasma processes, such as particle acceleration or Landau damping, that are beyond the scope of a fluidistic framework and require a more fundamental theoretical description.

Acknowledgements: Dr. Sersic was undoubtedly one of the most prestigious astronomers in Argentina. It is therefore an immense honor to receive the *Jose Luis Sersic* award to Senior Researchers. I feel greatly indebted to the *Asociación Argentina de Astronomía* for granting me this award, To my advisors, Dr. Virpi Niemela (graduation thesis) and Dr. Constantino Ferro Fontán (PhD thesis), I am really thankful for their guidance and support in the early stages on this journey. I am also specially grateful to the public education system in Argentina, of which I am one of the very many proud beneficiaries.

The research presented here has been supported by grants PICT 1707/2015 from the Agencia Nacional de Promoción de Ciencia y Tecnología (Argentina) and UBACyT 20020130100629BA/2014 from the University of Buenos Aires (Argentina).

References

Andrés N., et al., 2014a, Physics of Plasmas, 21, 072904
Andrés N., et al., 2014b, Physics of Plasmas, 21, 122305
Andrés N., Dmitruk P., Gómez D., 2016a, Physics of Plasmas, 23, 022903
Andrés N., et al., 2016b, Phys. Rev. E, 93, 063202
Balogh A., Treumann R. A., 2013, Physics of Collisionless Shocks: Space Plasma Shock Waves, ISSI Scientific Report Series, Volume 12. ISBN 978-1-4614-6098-5. Springer Science+Business Media New York, 2013
Foullon C., et al., 2011, ApJ, 729, L8
Gómez D. O., Mininni P. D., Dmitruk P., 2005, Phys. Scripta Vol. T, 116, 123
Gómez D. O., Mahajan S. M., Dmitruk P., 2008, Physics of Plasmas, 15, 102303
Gómez D. O., Martín L. N., Dmitruk P., 2013, Adv. Space Res., 51, 1916
Gómez D. O., Bejarano C., Mininni P. D., 2014, Phys. Rev. E, 89, 069906
Gómez D. O., DeLuca E. E., Mininni P. D., 2016, ApJ, 818, 126
Gómez D. O., 1990, Fund. Cosmic Phys., 14, 131
Gómez D. O., 2009, Compact Objects and Their Emission. Asociación Argentina de Astronomía, Book Series, vol. 1, pp 123–146
Mazelle C., et al., 2010, Twelfth International Solar Wind Conference, 1216, 471
Ofman L., Thompson B. J., 2011, ApJ, 734, L11
Parker E. N., 1957, J. Geophys. Res., 62, 509
Sahraoui F., et al., 2009, Physical Review Letters, 102, 231102
Schwartz S. J., et al., 2011, Physical Review Letters, 107, 215002
Velazquez P. F., et al., 1998, A&A, 334, 1060
von Karman T., Howarth L., 1938, Proceedings of the Royal Society of London Series A, 164, 192